THE JOURNAL OF BIOLOGICAL CHEMISTRY VOL. 289, NO. 26, pp. 17960–17969, June 27, 2014
Published in the U.S.A.

Proteolytic Degradation of Topoisomerase II (Top2) Enables the Processing of Top2·DNA and Top2·RNA Covalent Complexes by Tyrosyl-DNA-Phosphodiesterase 2 (TDP2)*◆

Received for publication, March 14, 2014, and in revised form, April 30, 2014 Published, JBC Papers in Press, May 7, 2014, DOI 10.1074/jbc.M114.565374

Rui Gao[‡], Matthew J. Schellenberg[§], Shar-yin N. Huang[‡], Monica Abdelmalak[‡], Christophe Marchand[‡], Karin C. Nitiss[¶], John L. Nitiss[¶], R. Scott Williams[§], and Yves Pommier[‡1]

From the [‡]Laboratory of Molecular Pharmacology, Center for Cancer Research, NCI, National Institutes of Health, Bethesda, Maryland 20892, the [§]Laboratory of Structural Biology, NIEHS, National Institutes of Health, Research Triangle Park, North Carolina 27709, and the [¶]Department of Biopharmaceutical Sciences, College of Pharmacy, University of Illinois, Rockford, Illinois 61107

Background: TDP2 is critical for repairing Top2 cleavage complexes (Top2cc) and as the VPg unlinkase for picornavirus replication.
Results: Top2 proteolysis or denaturation is required for TDP2 activity. TDP2 also hydrolyzes Top2cc at ribonucleotides.
Conclusion: TDP2 efficiently disjoints relatively large Top2 polypeptide-DNA and -RNA complexes.
Significance: Top2 processing is critical prior to its unlinking from DNA or RNA by TDP2.

Eukaryotic type II topoisomerases (Top2α and Top2β) are homodimeric enzymes; they are essential for altering DNA topology by the formation of normally transient double strand DNA cleavage. Anticancer drugs (etoposide, doxorubicin, and mitoxantrone) and also Top2 oxidation and DNA helical alterations cause potentially irreversible Top2·DNA cleavage complexes (Top2cc), leading to Top2-linked DNA breaks. Top2cc are the therapeutic mechanism for killing cancer cells. Yet Top2cc can also generate recombination, translocations, and apoptosis in normal cells. The Top2 protein-DNA covalent complexes are excised (in part) by tyrosyl-DNA-phosphodiesterase 2 (TDP2/TTRAP/EAP2/VPg unlinkase). In this study, we show that irreversible Top2cc induced in suicidal substrates are not processed by TDP2 unless they first undergo proteolytic processing or denaturation. We also demonstrate that TDP2 is most efficient when the DNA attached to the tyrosyl is in a single-stranded configuration and that TDP2 can efficiently remove a tyrosine linked to a single misincorporated ribonucleotide or to polyribonucleotides, which expands the TDP2 catalytic profile with RNA substrates. The 1.6-Å resolution crystal structure of TDP2 bound to a substrate bearing a 5′-ribonucleotide defines a mechanism through which RNA can be accommodated in the TDP2 active site, albeit in a strained conformation.

Human type II topoisomerases (Top2α and Top2β) resolve DNA catenanes, knots, tangles, and superhelical tension generated during DNA replication, transcription, and chromatin remodeling. Top2 enzymes catalyze these essential reactions by introducing transient DNA double strand breaks through covalent bonding of the catalytic tyrosine from each homodimer subunit to the 5′-ends of the DNA backbone at the break site (see scheme in Fig. 1*B*) (1–7).

Top2 cleavage complexes (Top2cc)[2] are the target of clinically important anticancer drugs, including etoposide, doxorubicin and mitoxantrone (3, 6–8). When one such drug binds in the catalytic site of Top2 at the enzyme-DNA interface (9–12), it misaligns the cleaved DNA ends, interfering with the religation step, thereby trapping Top2 on DNA and killing cancer cells (9–12). At the same time, however, drug-induced Top2cc form in normal cells, damaging their DNA and inducing apoptosis, which accounts for the dose-limiting toxicity of Top2 inhibitors. In addition, Top2cc in normal cells occasionally give rise to translocations, which cause secondary malignancies, specifically therapy-related acute myeloblastic leukemias (7, 13, 14). Dietary flavonoids trap Top2cc as well (7, 15–18) and have been implicated as a cause of infant leukemia (19). In addition, Top2cc can be stimulated by Top2 oxidation (3, 7, 20) and by the presence of a ribonucleotide incorporated in DNA (21). Recent evidence indicates that ribonucleotide incorporations into the genome are much higher than other endogenous or carcinogenic base damages (up to 1,000,000 ribonucleotides per mouse genome (22) and 10,000 per cell cycle in budding yeast (23)). Thus, it is plausible that stabilized Top2cc form at ribonucleotide-containing sequences, uncoupling the cleavage and resealing reactions. Based on the broad circumstance under which Top2cc can accumulate, their repair is a critical process impacting therapeutic response and resistance to Top2 inhibitors (24), as well as Top2cc-induced side effects, genotoxicity, and carcinogenesis.

How Top2·DNA covalent complexes are processed is under active investigation. Human tyrosyl-DNA-phosphodiesterase 2

* This work was supported, in whole or in part, by National Institutes of Health Grant Z01 BC 006150 from NCI Intramural Program, Center for Cancer Research, Grant R01 CA52814 from NCI Extramural Program (to J. L. N.), Grant 1Z01ES102765 from NIEHS (to R. S. W.).
◆ This article was selected as a Paper of the Week.
The atomic coordinates and structure factors (code 4PUQ) have been deposited in the Protein Data Bank (http://wwpdb.org/).
[1] To whom correspondence should be addressed: Developmental Therapeutics Branch, Center for Cancer Research, NCI, National Institutes of Health, Bethesda, MD 20892. Tel.: 301-496-5944; Fax: 301-402-0752; E-mail: pommier@nih.gov.

[2] The abbreviation used is: Top2cc, Top2 cleavage complex.

(TDP2) was recently discovered as the repair enzyme for Top2cc (24) and possibly Top3cc (25). TDP2 hydrolyzes 5′-tyrosine phosphodiester bonds, converting them into 5′-phosphate ends ready for religation. *In vitro* studies show that TDP2 can resolve phosphotyrosine bonds, even when a bulky adduct (*e.g.* a digoxigenin) is attached to the tyrosine, revealing the potential of TDP2 to hydrolyze tyrosyl-DNA bonds even when a peptide is attached to the tyrosine (25). Yet crystal structures show that TDP2 has a relatively tight catalytic site (26, 27), suggesting Top2 might need to be proteolyzed or denatured for TDP2 to access the tyrosyl-DNA bond. Accordingly, cellular studies indicate that the 26 S proteasome is involved in the degradation of stabilized Top2cc (28, 29). However, it remains unproven whether Top2 degradation is necessary for the resolution of the protein-DNA adduct by TDP2.

To investigate how stabilized Top2cc are approached and processed by TDP2, we took advantage of the trapping of Top2 by suicidal substrates (Fig. 1) (21, 30) and studied the conditions required for the processing of trapped Top2cc by TDP2 *in vitro*. Additionally, we tested whether TDP2 can resolve Top2 trapped by a ribonucleotide in the DNA complex. Furthermore, we report a crystal structure of TDP2 bound to an RNA-DNA junction that illuminates the molecular basis for processing of 5′-phosphotyrosine-adducted RNA-DNA junctions.

MATERIALS AND METHODS

Purification of Recombinant Proteins—Recombinant TDP2 was produced in baculovirus by SAIC (Frederick, MD). A truncated version of the yeast Top2 (yTop2(410–1202)) protein (from amino acids 410–1202) was kindly provided by James Berger, University of California, Berkeley.

5′-Linked Peptidyl Substrate Preparation and TDP2 Reactions—The 5′-linked peptidyl substrates were prepared as described previously (31), with some modifications as detailed below. Ten pmol of the top strand oligonucleotide (T18, shown in Table 1) was end-labeled with 3′-deoxyadenosine 5′-triphosphate (3′-[α-^{32}P]cordycepin 5′-triphosphate) (PerkinElmer Life Sciences) using terminal deoxynucleotidyltransferase (Invitrogen). The labeled oligonucleotide was purified from unincorporated nucleotide on a mini-quick spin oligonucleotide column (Roche Applied Science) and annealed with 10 pmol of the bottom strand oligonucleotide (B30, containing a 3-carbon spacer at the 3′ terminus) by heating to 95 °C for 2 min followed by cooling to room temperature overnight in a buffer containing 10 mM Tris-Cl, pH 7.4, 2.5 mM $MgCl_2$, 2.5 mM $CaCl_2$, 20 mM NaCl, 15 μg/ml BSA, 0.5 mM EDTA, pH 8.0. The yTop2(410–1202) enzyme was incubated with the annealed, labeled oligonucleotides at a 5:1 protein to DNA molar ratio for 1 h at 30 °C. To generate the trypsinized substrate, trypsin (Sigma) was added to a final concentration of 3 mg/ml, and the reaction was incubated overnight at 37 °C. The sequences of oligonucleotides are listed in Table 1. Equal amounts of intact, trypsin-treated, or denatured 5′-linked peptidyl substrates were incubated with 10 nM TDP2 at 25 °C for 30 min.

Preparation of DNA Substrates and in Vitro TDP2 Reactions—Oligonucleotides with 5′-phosphotyrosine linkage were synthesized by The Midland Certified Reagent Co. (Midland, TX). All other oligonucleotides were synthesized by Integrated DNA Technologies (Coralville, IA). In addition, the 5′-Y-RNA substrate and the corresponding control 5′-Y-DNA substrate (5′-Y-rUrUrArArArArCrArGrC and 5′-Y-TTAAAACAGC, a kind gift from Dr. John Tainer, Lawrence Berkeley National Laboratory, Berkeley, CA) were ligated to a 5′-^{32}P-labeled hairpin oligonucleotide (5′-p*-GCTTACGATTGCTTTTGCAA-TCGTAAGCGCTGTT). The markers bearing 5′-phosphate instead of 5′-Y were prepared the same way. Detailed description of the biochemical reaction is provided previously (25). Briefly, 1 nmol of labeled DNA substrate in a 10-μl reaction volume was incubated with 10 nM recombinant human TDP2 unless otherwise indicated for 30 min at room temperature in TDP2 reaction buffer. Reactions were terminated by adding 1 volume of gel loading buffer (99.5% (v/v) formamide, 5 mM EDTA, 0.01% (w/v) xylene cyanol, 0.01% (w/v) bromphenol blue, and 5 mM EDTA). Samples were subjected to 16% denaturing PAGE. Gels were dried and exposed on PhosphorImager screens. Imaging and quantification were done using a Typhoon 8600 (GE Healthcare) and ImageJ software (National Institutes of Health, Bethesda). Results shown in figures are representative of at least three independent experiments.

TABLE 1
Oligonucleotides used in this study

Oligonucleotide name	Sequence
T18	5′-TATATATACATTTATATA-3′
B30	5′-GGTTATATAAATGTATATATAGGAGATCAG-3′
p15 (marker)	5′-(p)ATATACATTTATATA-3′
riboB30	5′-GGTTATATAAATGTrATATATAGGAGATCAG-3′
Y-18	5′-tyrosine-TCCGTTGAAGCCTGCTTT-3′
Y-ribo-18	5′-tyrosine-UCCGTTGAAGCCTGCTTT-3′
B15	5′-TAAAGCAGGCTTCAA-3′
B19	5′-TAAAGCAGGCTTCAACGGA-3′
B23	5′-TAAAGCAGGCTTCAACGGAGCCA-3′
B40	5′-TAAAGCAGGCTTCAACGGAGCCATCCGCCGCTAGCTGCGC-3′
T17 (B40)	5′-GCGCAGCTAGCGGCGGA-3′
T21 (B40)	5′-GCGCAGCTAGCGGCGGATGGC-3′

TDP2-RNA·DNA Complex Crystallization—Expression of the mouse TDP2 catalytic domain (mTdp^{cat} residues 118-370) for crystallization was carried out as described (26). The TDP2-RNA·DNA complex was crystallized using a dual one nucleotide 5′-overhang crystallization strategy (26) and a 5′-phosphorylated self-annealing oligonucleotide. Crystals of mTDP2-RNA·DNA complex were grown by sitting drop vapor diffusion in TTP LabTech 96-well crystallization trays and mixing 200 nl of TDP2-RNA·DNA complex (9.0 mg/ml mTdp^{cat}, 1.2:1 protein/nucleic acid molar ratio in 200 mM NaCl, 10 mM Tris, 7.5, 4 mM TCEP, 4 mM $MgCl_2$) with 200 nl of precipitant solution (20% PEG 3350, 200 mM sodium acetate). Crystals that grew within 1–2 days were transferred to a cryoprotectant solution (Cryo 25% PEG 3350, 12% glycerol, 100 mM sodium acetate, 5 mM magnesium acetate) immediately prior to flash freezing in liquid nitrogen.

Crystallographic Data Processing and Refinement—X-ray data were collected at the Advanced Photon Source beamline 22-ID (SER-CAT) and processed with HKL2000. RNA-DNA-bound mTDP2 structure was phased by molecular replacement with the DNA-bound TDP2 reaction product complex structure (RCSB 4GZ1 (26)). Molecular replacement and refinement were conducted in PHENIX. The final model displays excellent geometric and refinement parameters (Table 2).

TABLE 2

X-ray data collection and refinement statistics

All data were collected from a single crystal. Values in parentheses are for highest resolution shell.

Data collection	mTdp2^{cat}-RNA/DNA
Space group	$P2_12_12_1$
Cell dimensions	
a, *b*, *c*	54.83, 69.26, 167.11 Å
α, β, γ	90, 90, 90°
Resolution	50 to 1.60 Å (1.66 to 1.6 Å)
R_{sym} or R_{merge}	0.061 (0.548)
$I/\sigma I$	19.5 (2.0)
Completeness	98.1% (89.1%)
Redundancy	3.5 (2.7)
Wilson B-factor	19.0
Refinement	
Resolution	50 to 1.60 Å
No. of reflections	81,926
Minimum $F/\sigma F$	1.35
R_{work}/R_{free}	0.140/0.179
No. of atoms	
Protein	4,360
Ligand/ion	482
Water	662
B-factors	
Protein	25.4
Ligand/ion	45.0
Water	43.0
Ramachandran plot	
Favored	98.6%
Allowed	1.4%
Outliers	0%
Root mean square deviations	
Bond lengths	0.008 Å
Bond angles	1.21°

RESULTS

TDP2 Processes Proteolyzed Top2cc but Not Top2cc with Full-length Native Top2—To generate a Top2 peptidyl-DNA substrate for TDP2 processing, we used a suicide cleavage substrate containing a high affinity Top2 recognition sequence (21). The Top2 substrate was designed as an 18-nucleotide 5′-recessed top strand with three nucleotides 5′ to the cleavage site and a 30-nucleotide-long bottom strand (Fig. 1, *A* and *B*). Upon Top2-mediated cleavage, the trinucleotide at the 5′-end of the top strand is released (Fig. 1*C*), leaving a Top2 molecule covalently linked to the DNA substrate. Moreover, cleavage of the lower strand can also generate a suicide complex with the release of the lower strand segment 5′ from the Top2 cleavage site (Fig. 1*C*, *bottom*).

We first explored the processing of the top strand suicide product by TDP2 (Figs. 2 and 3). As expected, Top2-linked DNA cleavage resulted in a retarded mobility of the 3′-labeled oligonucleotide due to the covalent bonding of Top2 to the 5′-end of the DNA. The polypeptide-oligonucleotide band was visible in the well of 16% polyacrylamide gels (representative experiment shown in Fig. 2*A*, *lane 2*).

In the absence of proteolytic digestion, the Top2·DNA suicide complex was not processed by TDP2 (Fig. 2, *lane 3*). As expected, following trypsin digestion, the covalently linked Top2 was degraded into polypeptides of various length, resulting in the migration of Top2 peptide·DNA conjugates into the gel (bands numbered *i*–*iv* in Fig. 2, *A* and *B*). Concurrently, a small fraction of 19-mer reappeared, probably resulting from the reversal of some Top2cc under the trypsin digestion conditions (Figs. 2, *lanes 4* and *5*, and 1*C*). Following trypsin digestion, TDP2 converted all four Top2 peptide-DNA conjugates into the expected 16-mer oligonucleotide product (see Fig. 1*D*). These results demonstrate that proteolytic digestion of Top2 is required for optimal Top2cc processing by TDP2.

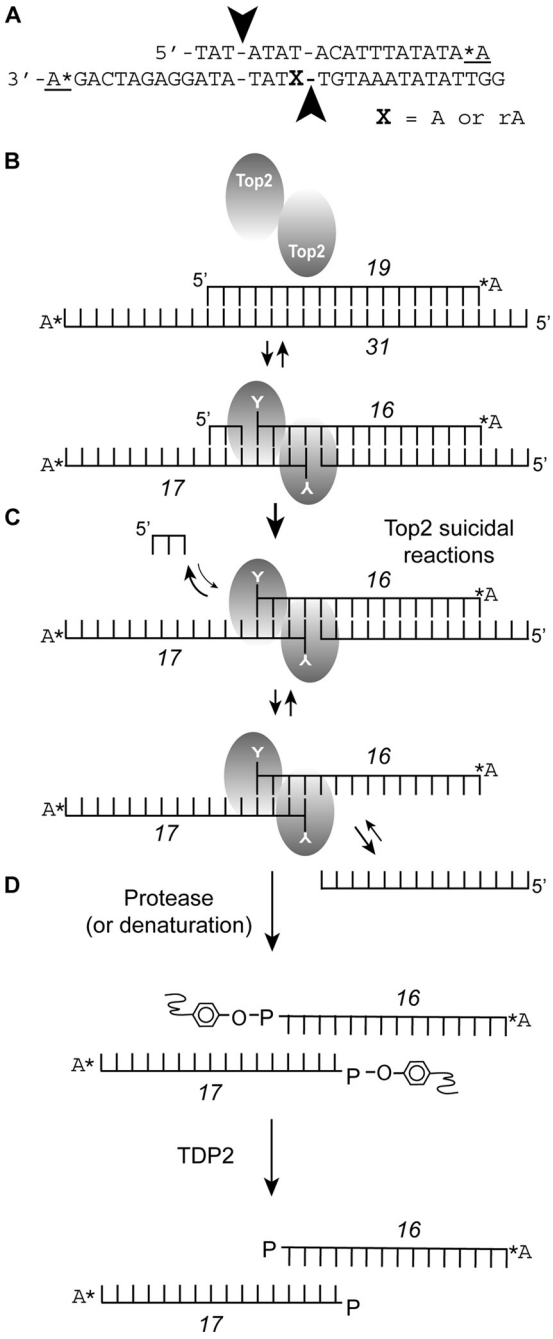

FIGURE 1. **Oligonucleotides used to study the processing of irreversible Top2 cleavage complexes (referred to as suicidal Top2cc) by TDP2.** *A*, sequence of the substrates. The *underlined* adenosines with *asterisks* denote ^{32}P-radioactive labeling of the 3′-end of either strand. *X* represents either a nucleotide or a ribonucleotide at the cleavage site of the *bottom strand* used to enhance Top2cc. *B*, illustration of the Top2cc. *C*, generation of suicidal Top2cc by dissociation of the three-nucleotide segment 5′ to the Top2 cleavage site on the *upper strand*. The *lower cleaved strand* can also potentially dissociate. *D*, TDP2 processing requires prior protease digestion or denaturation of the Top2cc. *Numbers* represent the length of the oligonucleotides (including the 3′-labeling with cordycepin: *A or A*. The Top2 active site tyrosines are represented as *Y*.

Trypsin is known to cleave at the C terminus of arginine or lysine residues. As shown in Fig. 2*D*, several arginines and

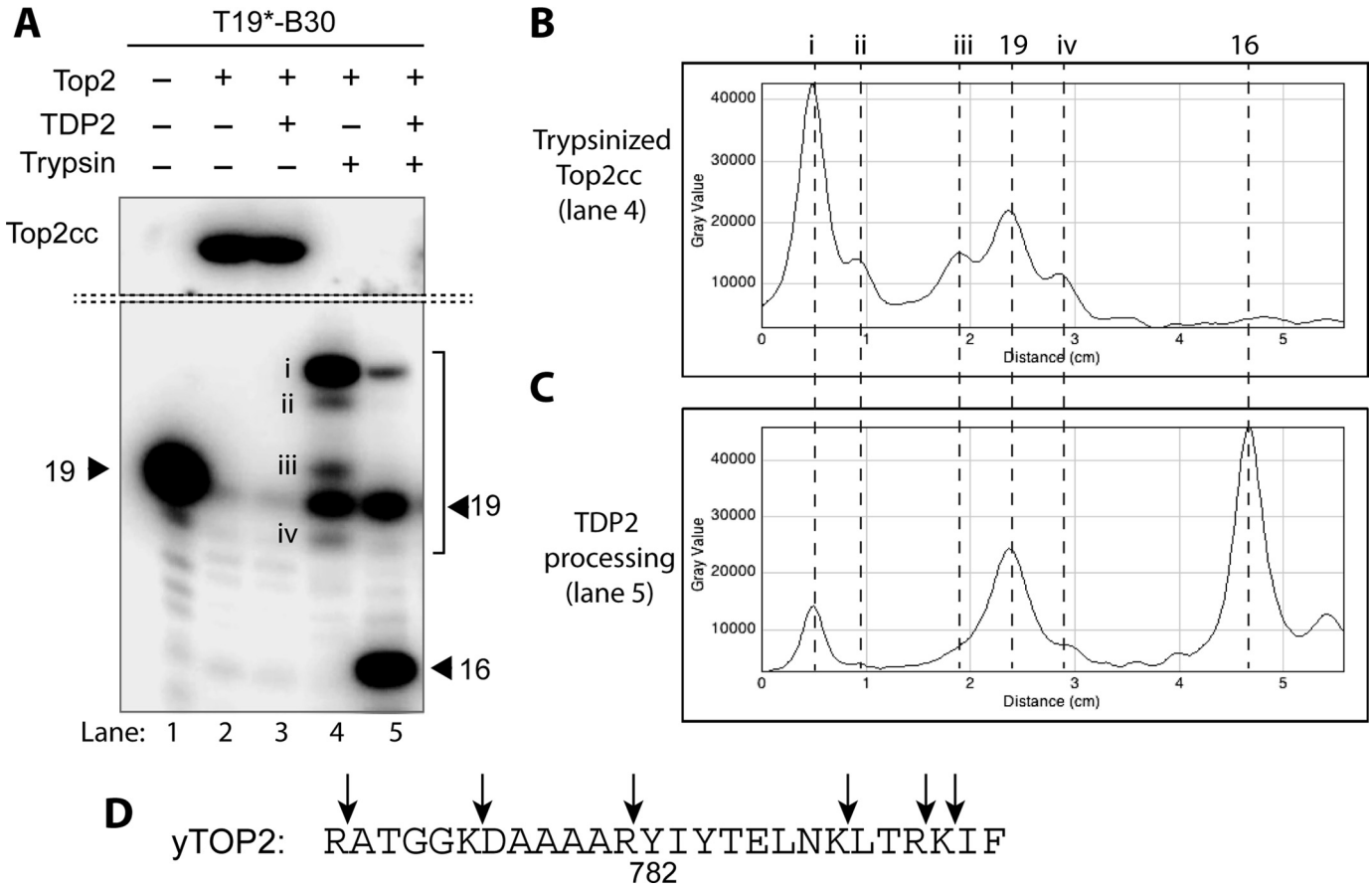

FIGURE 2. **Top2 proteolytic digestion allows the processing of trapped Top2cc by TDP2.** *A,* representative gel showing the processing of Top2cc by TDP2. The middle portion of the gel is not included (space between *dotted lines*) to limit the size of the figure (a full size gel is shown in Fig. 4*A*). The suicidal substrate labeled at the 3′-end of the *top strand* (19-mer) is described in Fig. 1. Top2 trapping on the DNA results in the retention of the labeled oligonucleotide in the well of the gel (*lane 2*). Native Top2cc is not processed by TDP2 (*lane 3*). Digestion of Top2cc with trypsin results in peptides of various lengths (*lane 4, bands i–iv* inside the *bracket*), which are processed by TDP2 into the expected 16-mer product (*lane 5*). *B* and *C,* quantitative representation of TDP2 processing of trypsin-digested Top2cc. *Peaks* in the graph correspond to the bands labeled in *A*. The *height* of each peak corresponds to the numbers of pixels for each band. *D*, sequence of yeast Top2 around the catalytic tyrosine 782, with *arrows* indicating tryptic cleavage sites.

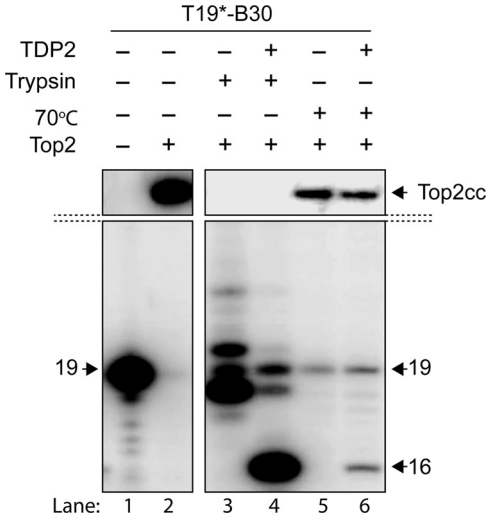

FIGURE 3. **Denaturation of Top2cc is sufficient for TDP2 processing.** Reactions and substrate are as in Fig. 2. A representative experiment is shown. The middle portion of the gel is not included (space between *dotted lines*) to limit the size of the figure (a full size gel is shown in Fig. 4*A*). *Lane 1,* oligonucleotide only; *lane 2,* trapped Top2cc; *lane 3,* tryptic digest of Top2cc (as in Fig. 2, *lane 4*); *lane 4,* TDP2 processing Top2cc digested by trypsin (as in Fig. 2, *lane 5*); *lane 5,* denaturation of Top2cc in the absence of TDP2; *lane 6,* TDP2 can process denatured Top2cc.

lysines surround the catalytic tyrosine of Top2. Therefore, it is likely that the smallest oligopeptide band *iv* shown in Fig. 2, *A–C,* corresponds to Top2 peptides consisting of ≥8 amino acids. Based on the tryptic map (Fig. 2*D*), it is plausible that the major tryptic band (i) includes more than 12 amino acid residues. Nevertheless, all the peptide·DNA complexes, including the largest band (i) were readily processed by TDP2, indicating that TDP2 can hydrolyze DNA·Top2 polypeptides of various length without the need for Top2 to be proteolyzed to a single tyrosyl-5′-end.

TDP2 Processes Heat-denatured Top2cc but Less Efficiently than Proteolyzed Top2cc—To test whether TDP2 needs proteolytic digestion of Top2 and whether it can process denatured Top2cc, the trapped Top2cc were heated at 70 °C for 10 min before TDP2 treatment. Such heat denaturation allowed TDP2 to process Top2cc with the release of the protein-free oligonucleotide product (16-mer, Fig. 3, *lane 6*). However, the efficiency of TDP2 was limited compared with proteolytic digestion, with only a small fraction of the Top2cc converted to the 16-mer product (Fig. 3, compare *lanes 6* and *4*). These results demonstrate that TDP2 is able to process denatured Top2cc in the absence of proteolysis.

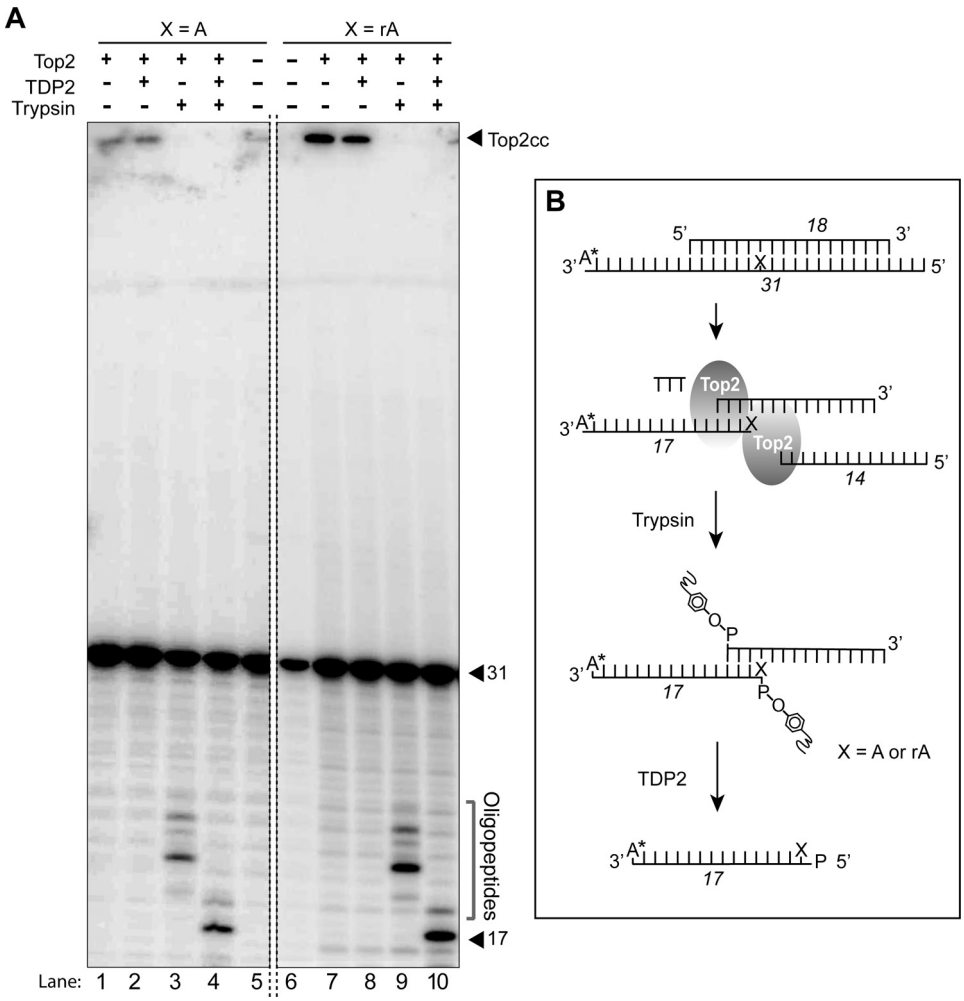

FIGURE 4. **TDP2 can remove Top2 bonded to a ribonucleotide.** *A,* representative gel showing the processing of Top2 trapped at a ribonucleotide site (see Fig. 1 and *B*). Trypsin generates various length oligopeptides (indicated by the *bracket*). *B,* schematic representation of the reactions. The *bottom strand* was labeled at the 3′ terminus (see Fig. 1). Trypsin digestion generates single-stranded DNA with tyrosyl peptide covalently bound to the 5′ termini. TDP2 hydrolyzes the 5′-tyrosine phosphodiester bond, producing a 17-mer oligonucleotide with a 5′-phosphate.

Ribonucleotide Incorporation Enhances Irreversible Top2cc but Does Not Preclude Hydrolysis of the 5′-Tyrosyl RNA Phosphodiester Bond by TDP2—Because of the high frequency of ribonucleotide incorporation in the genome (see Introduction and under "Discussion"), and based on prior biochemical evidence that the cleavage activity of Top2 can be stimulated by ribonucleotide-containing substrates (21), we asked whether TDP2 can process Top2cc trapped by ribonucleotide incorporation at a Top2 cleavage site. To address this question, we used the suicidal substrate shown in Fig. 1 after insertion of a ribonucleotide at the cleavage site of the bottom strand (riboB30, Table 1; Figs. 1*A* and 4*B*). The bottom strand was labeled at the 3′-end (as illustrated in Figs. 1*A* and 4*B*). As expected, the Top2 cleavage activity was stimulated by the ribonucleotide-containing substrate (Fig. 4*A*, compare *lanes 6* and *7 versus 1* and *5*) (21). Consistent with the top strand results (see Figs. 2 and 3), trypsin generated a mixture of peptide-DNA conjugates of various lengths, which are indicated by the *bracket* in Fig. 4*A*. Following trypsin digestion, both the deoxynucleotide- and ribonucleotide-containing substrates were processed by TDP2 into the expected 17-mer product (see Figs. 4*B* and 1*D*, *bottom*). Yet, consistent with the top strand results (see Figs. 2 and 3), native Top2cc resisted TDP2 processing (Fig. 4*A*, *lanes 2* and *8*).

DNA and RNA Substrate Preference of TDP2—To compare the efficiency of TDP2 on both 5′-deoxyribose and 5′-ribose substrates, we measured the activity of TDP2 using single-stranded 19-mer oligonucleotides (25) with either a single 5′-ribonucleotide or the corresponding deoxyribonucleotide linked to the tyrosine (see *upper schemes* in Fig. 5*A*). TDP2 processed both substrates but exhibited a greater efficiency for the substrate bearing the 5′-deoxyribonucleotide than the one bearing a single ribonucleotide (Fig. 5, *A* and *B*).

To further examine the differential processing of deoxyribonucleotides *versus* ribonucleotide substrates, we designed two comparable oligonucleotides with either 10 consecutive ribo- or deoxyribonucleotides linked to the 5′-tyrosine (Fig. 5*C*, *upper schemes*). Both were processed by TDP2 (Fig. 5, *C, bottom,* and *D*). However, as in the case of the single 5′-ribonucleotide (see Fig. 5, *A* and *B*), processing was more efficient for the deoxyribonucleotide substrate (Fig. 5, *C* and *D*).

Top2-mediated double strand break reactions can be uncoupled by various DNA lesions and drugs, resulting in asymmet-

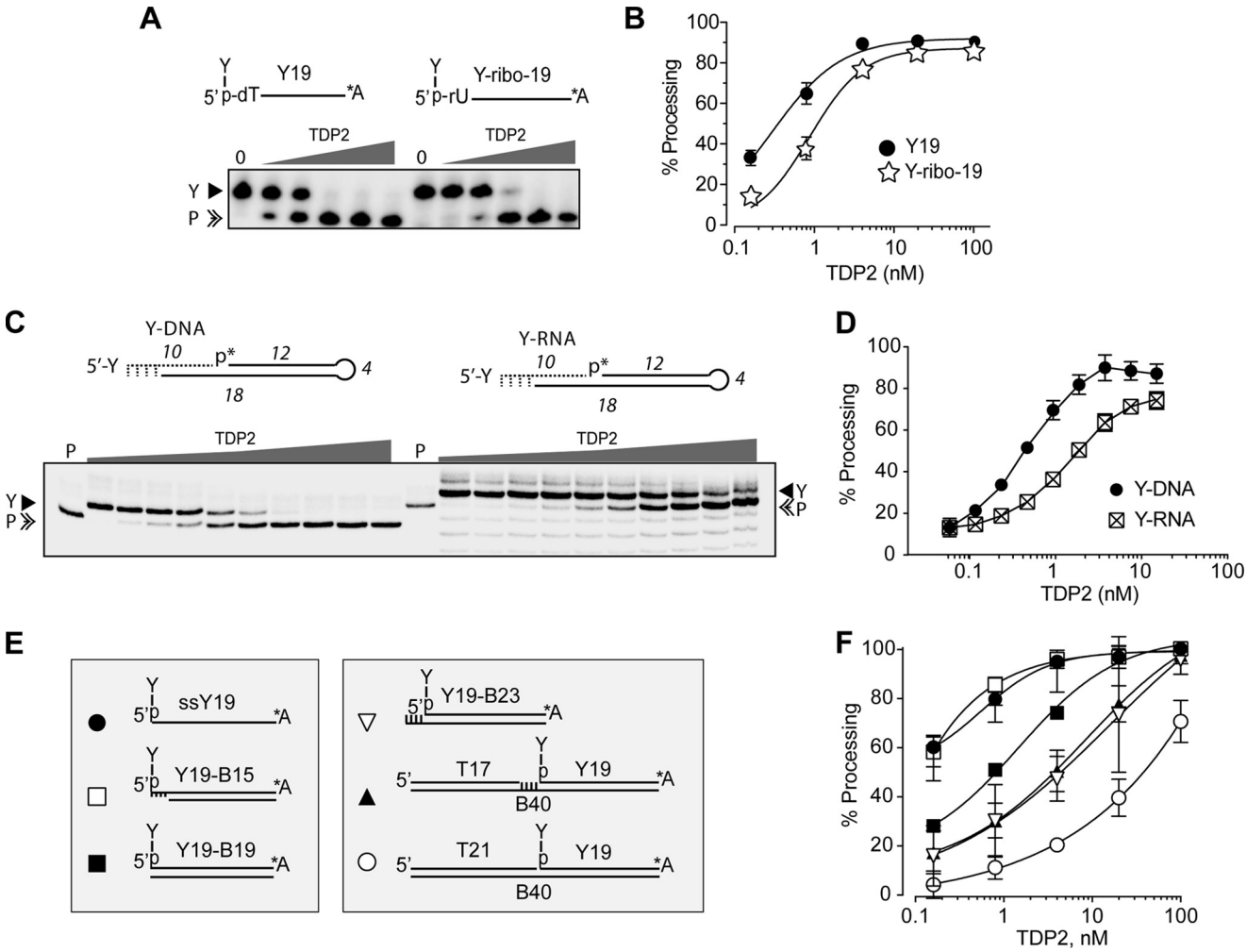

FIGURE 5. **DNA and RNA substrate structure dependence for TDP2.** *A,* processing of a single-stranded 19-mer oligonucleotide (25) bearing a 5′-tyrosine linked to a deoxythymidylate (*left*) or uridine monophosphate (*right*). Oligonucleotides were incubated at 25 °C for 30 min with increasing TDP2 concentrations from 016 to 100 nM in 4-fold increments. *Y* and *P* represent the TDP2 substrates and products, respectively. *B,* quantitation based on three independent experiments. *C,* processing of the oligonucleotides represented *above* each gel. The tyrosine was attached to the 5′-end of either 10 deoxyribonucleotides (*left*) or 10 ribonucleotides (*right*). The last four nucleotides were unpaired (*dotted lines*). *Y* and *P* represent the TDP2 substrates and products, respectively. TDP2 concentrations ranged from 0.06 to 15 nM in 2-fold increments. *D,* quantitation based on three independent experiments. *E,* DNA substrates used to determine that TDP2 preferentially acts on accessible 5′-tyrosyl ends as follows: single-stranded DNA (*closed circle*), double-stranded DNA with 4-base overhang at the 5′-end (*open square*), blunt-ended double-stranded DNA (*closed square*), double-stranded DNA with a 4-base recessed end (*open triangle*), double-stranded DNA with a 4-base gap next to the tyrosine (*closed triangle*), or double-stranded DNA with a nick next to the tyrosine (*open circle*). *F,* quantitation from ≥3 independent experiments. The optimal DNA substrates have open phosphotyrosine bonds. Tyrosine at a nick in the middle of a double-stranded DNA is the least processed.

rical Top2cc in which only one DNA strand is cleaved at any given time (8, 32, 33). Therefore, the tyrosine from a trapped topoisomerase can be linked to different types of DNA ends. Fig. 5*E* summarizes various DNA configurations where Top2 potentially can be irreversibly stabilized. Our single-stranded substrate (Fig. 5*E, filled circle*) was used as in Ref. 25. The blunt end duplex DNA (Fig. 5*E, filled square*) was also included because it was used in the seminal study describing the biochemical activity of TDP2 (24), although it is unlikely to be formed by Top2 because Top2 homodimers cleave both DNA strands with a canonical 4-base 5′-overhang (1–3, 6). Comparing the substrates shown in Fig. 5 provides insights into TDP2 substrate preference. The double-stranded physiological substrate with the 4-base 5′-overhang (*open squares*, Fig. 5, *E* and *F*) was as efficiently processed by TDP2 as the single-stranded substrate (Fig. 5*F*). As expected (24), the substrate with a blunt end (*filled squares*) was also processed, although less efficiently. In the cases where the 5′-tyrosine was attached to a recessed end or gap (*open* and *closed triangles*; Fig. 5, *E* and *F*), the efficiency decreased ~100-fold, compared with single-stranded DNA. Finally, when the tyrosine was immediately adjacent to a DNA nick, TDP2 displayed very low activity (*open circles*; Fig. 5*F*). These results are consistent with the crystal structures for TDP2, showing the enzyme has a narrow DNA binding pocket, optimal for accessing single-stranded DNA ends (26, 27).

Crystal Structure of a TDP2-RNA/DNA Junction—To define the molecular basis for TDP2 processing of Top2 adducted RNA-DNA junctions, we crystallized and determined a 1.60 Å structure of mouse TDP2 bound to a 5′-RNA-DNA-3′ junction, as a 5′-phosphorylated reaction product complex state (Fig. 6). Overall, the structure reveals that the ribonucleotide-containing substrate binds in the TDP2 active site in a manner

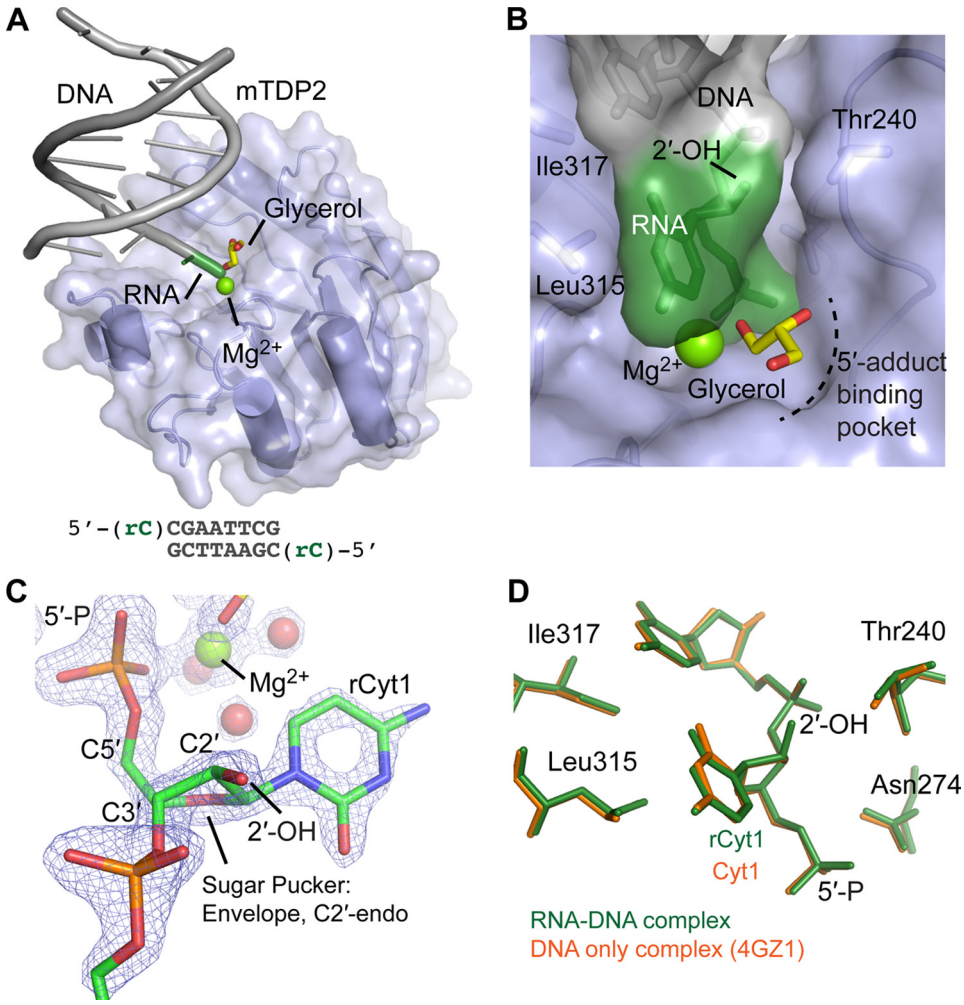

FIGURE 6. **X-ray structure of mouse TDP2 bound to an RNA-DNA junction.** *A,* RNA-DNA 5′ terminus is engaged in the active site of TDP2. The 5′-ribonucleotide (rCytl, *green tube*) and DNA (*gray tube*) are displayed on a surface representation of TDP2 (*blue*). *B,* active site surface representation of the TDP2-RNA/DNA junction interactions. van der Waals interactions from Thr-240 to the RNA secure the 5′-ribonucleotide in a C2′-endo conformation. The RNA is shown in *green*, with DNA in *gray*, and overlaid upon the TDP2 surface (*blue*). A glycerol (*yellow*) molecule is coordinated to the active site Mg^{2+} and occupies the expected position of leaving group Top2 active site tyrosine. *C,* σ-A weighted omit $2F_o - F_c$ electron map contoured at 2.5 σ shows clear electron density for the 2′-hydroxyl on of the 5′-ribonucleotide rCyt1. The ribose sugar is bound to TDP2 with a strained C2′-endo pucker conformation. *D,* structural overlay of TDP2 bound to RNA-DNA (displayed as *green sticks*) and the DNA-only complex (RCSB 4GZ1, displayed as *orange sticks*). RNA-DNA is bound in a similar manner to the DNA·RNA complex.

analogous to that observed for TDP2·DNA complexes (Fig. 6, *A–D*). Structural results show TDP2 utilizes a similar substrate-binding mode for tyrosyl DNA adduct processing in the context of DNA or RNA-DNA (Fig. 6*D*). In addition to the RNA-DNA, a solvent glycerol molecule from the crystallographic cryoprotectant binds in the TDP2 5′-adduct binding groove (Fig. 6, *A* and *B*). The glycerol hydroxyl moiety ligands a single octahedral coordinated Mg^{2+} ion and occupies the expected position of the enzymatic reaction product tyrosine hydroxyl, following tyrosyl phosphodiesterase cleavage (Fig. 6, *B* and *C*).

An array of protein RNA-DNA contacts to the 5′-terminal RNA-DNA secures the nucleic acid in the narrow TDP2 single strand DNA binding cleft (Fig. 6*A*). Tight interactions of the 5′-end with the walls of the active site secure the sugar phosphate backbone in an orientation appropriate for catalysis within the active site of TDP2, analogous to that proposed for an all-deoxy substrate (Fig. 6*D*) (26). Electron density for the 5′-rCyt1 nucleotide is unambiguous (Fig. 6*C*). To accommodate the 5′-ribonucleotide, the 5′-ribose sugar is bound in a strained conformer for RNA with an envelope, C2′-endo sugar pucker (Fig. 6*C*). Seven residues (Leu-315, Thr-240, Arg-276, Ser-239, Phe-325, Asp-272, and Asn-274) engage 5′-rCyt1 (Fig. 7). Close van der Waals interactions of the 5′-rCyt1 2′-hydroxyl with Thr-240 of the TDP2 active site "Cap" 3_{10}-helix substrate interaction motif stabilize the strained sugar conformer (Figs. 6*B* and 7). Although the RNA-DNA substrate binding mode is optimal for detyrosylation, this strained conformer also acts in precluding active site alignment of the terminal 2′-OH in a conformation that could be activated for attack on the adjacent 3′-phosphate in a 2′–3′ cyclization reaction within the TDP2-active site. We hypothesize the enzyme-induced steric strain of the 5′-ribose explains an ~3-fold reduced activity on RNA-containing substrates (Fig. 5, *A–D*).

DISCUSSION

Eukaryotic DNA topoisomerases II are essential for numerous DNA transactions, which all depend on the ability of the Top2 enzymes to introduce transient breaks in the

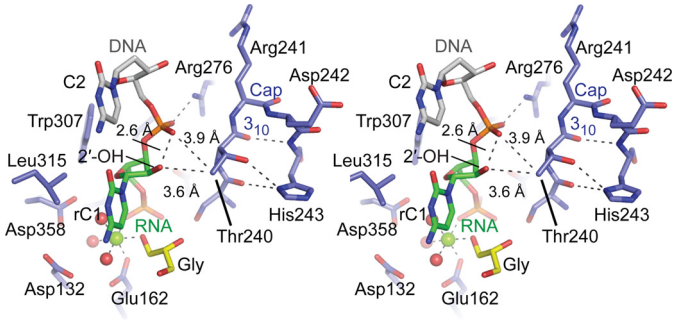

FIGURE 7. **TDP2 RNA·DNA complex interactions.** A stereo view of the TDP2-RNA·DNA complex. The 5′-RNA (*green sticks*) is positioned by interactions with the substrate binding "Cap" motif 3_{10} helix. van der Waals interactions between ribonucleotide 2′-OH and Thr-240 (*blue sticks*, side chain, Cγ2) orients the substrate and stabilizes a strained C2′-endo conformation of the terminal ribonucleotide.

DNA backbone (2). Yet, while doing so, Top2 enzymes can be trapped on DNA by endogenous DNA modifications, protein oxidation, food products, and anticancer drugs (1, 6, 7, 20, 34, 35), which explains why human cells have evolved mechanisms to remove such Top2-associated lesions. Previous reports have linked the proteasome pathway to the degradation of Top2 in response to Top2 inhibitors (28, 29). However, the mechanistic link between Top2 degradation and the repair of Top2-mediated DNA damage has not been formally established.

In this study, using a suicidal DNA substrate to trap Top2 cleavage complexes, we demonstrate that native Top2 cleavage complexes cannot be processed by TDP2 unless they are first proteolyzed or denatured. Our data demonstrate that proteolytic digestion of Top2 enables the hydrolysis of the Top2·DNA covalent linkage by TDP2 (see *scheme* in Fig. 1). In addition, we show that denaturation of Top2 can also, albeit much less efficiently, enable the processing of Top2cc by TDP2. These results provide the first mechanistic evidence linking directly Top2 degradation to the repair of Top2-induced DNA damage. The fact that Top2 polypeptides resulting from partial tryptic digestion were processed by TDP2 (see Figs. 2 and 4) and that mild Top2 denaturation (70 °C heating) (see Fig. 3) also allowed TDP2 action indicates that the active catalytic site of TDP2 can accommodate relatively large polypeptides (26, 27). This result is in line with the fact that TDP2 can process some substrates with a bulky 5′-tyrosyl end (25) and acts as the VPg unlinkase for picornavirus replication (36). However, the fact that a nicked duplex DNA substrate, which was designed to limit the space 5′ to the tyrosyl linkage portion, was refractory to TDP2 (see Fig. 5, *E* and *F*) is consistent with the fact that the nucleic acid segment of the substrate attached to the tyrosyl needs to be single-stranded to optimally bind to the narrow nucleic acid groove inside the TDP2 active site (26, 27).

Recent studies revealed that ribonucleotides can be incorporated into the genome at relatively high levels. In budding yeast, DNA polymerase ϵ incorporates one ribonucleotide for every 1,250 deoxyribonucleotides, whereas polymerase δ and α incorporate one ribonucleotide for every 5,000 or 625 deoxyribonucleotides, respectively (23). It has been estimated that more than 10,000 ribonucleotides may be incorporated into the nuclear genome during each round of replication in yeast. Likewise, human polymerase δ stably incorporates one ribonucleotide for ~2,000 deoxyribonucleotides (37), introducing more than a million ribonucleotides into the human genome per replication cycle. Thus, ribonucleotides may be the most common noncanonical nucleotides incorporated into the eukaryotic genome. Usually, this problem is taken care of by RNase H2-dependent repair, which, if defective, can result in replication stress, genomic instability, and an autoimmune disease (38). The genomic instability caused by ribonucleotides in DNA, in addition to their interference with Top1cc (39, 40), may be partially due to their toxic effect on Top2, as initially shown by Westergaard and co-workers (21). Our results confirm that the presence of a single ribonucleotide can increase Top2 cleavage complexes. Hence, it may be important for organisms to remove trapped Top2 cleavage complexes arising from RNA contamination in DNA. Here, we confirm that TDP2 is not only a tyrosyl-DNA phosphodiesterase but can also hydrolyze a 5′-tyrosine covalently linked to a ribonucleotide (see Fig. 4). The efficiency of TDP2 on a 5′-tyrosylated substrate with a single 5′-ribonucleotide or polyribonucleotide was slightly less than for the corresponding deoxyribonucleotide substrates (see Fig. 5). This difference can be accounted for by the differential binding and sugar pucker of ribonucleotide *versus* deoxyribonucleotide in the catalytic site of TDP2 (Figs. 6 and 7) (26, 27). Overall, the employment of the TDP2 direct DNA damage reversal mechanism to resolve 5′-adducts in the context of RNA is analogous to the repair of RNA-triggered 5′-adenylation damage repair by aprataxin (41). In the later case, aprataxin resolves 5′-AMP adducts (as compared with 5′-Top2 peptide adducts) generated when DNA ligases abortively process 5′-ribonucleotide-containing substrates.

Our study provides the first co-crystal structure of TDP2 bound to a tyrosyl-RNA substrate (see Figs. 6 and 7), which is relevant to the fact that TDP2 is not only associated with the repair of Top2 cleavage complexes (24) but has also been identified as the VPg unlinkase for picornaviruses, a large viral family including poliovirus, coxsackieviruses, rhinoviruses, and the classical foot-and-mouth disease virus (36). In closing, it is relevant to note that in type IA topoisomerases, the Top3 enzymes also form 5′-tyrosyl catalytic intermediates (2, 42). Thus, further studies are warranted to determine the potential relevance of TDP2 for the repair of Top3α·DNA and Top3β·DNA or RNA complexes (42–45).

Acknowledgments—We thank L. Pedersen of the National Institutes of Health, NIEHS, Collaborative Crystallography Group and the Advanced Photon Source (APS) Southeast Regional Collaborative Access Team (SER-CAT) for beamline access. Use of the Advanced Photon Source was supported by the United States Department of Energy, Office of Science, Office of Basic Energy Sciences, under Contract W-31-109-Eng-38.

REFERENCES

1. Nitiss, J. L. (2009) DNA topoisomerase II and its growing repertoire of biological functions. *Nat. Rev. Cancer* **9,** 327–337

2. Wang, J. C. (2002) Cellular roles of DNA topoisomerases: a molecular perspective. *Nat. Rev. Mol. Cell Biol.* **3,** 430–440
3. McClendon, A. K., and Osheroff, N. (2007) DNA topoisomerase II, genotoxicity, and cancer. *Mutat. Res.* **623,** 83–97
4. Schoeffler, A. J., and Berger, J. M. (2008) DNA topoisomerases: harnessing and constraining energy to govern chromosome topology. *Q. Rev. Biophys.* **41,** 41–101
5. Schoeffler, A. J., and Berger, J. M. (2005) Recent advances in understanding structure-function relationships in the type II topoisomerase mechanism. *Biochem. Soc. Trans.* **33,** 1465–1470
6. Pommier, Y., Leo, E., Zhang, H., and Marchand, C. (2010) DNA topoisomerases and their poisoning by anticancer and antibacterial drugs. *Chem. Biol.* **17,** 421–433
7. Deweese, J. E., and Osheroff, N. (2009) The DNA cleavage reaction of topoisomerase II: wolf in sheep's clothing. *Nucleic Acids Res.* **37,** 738–748
8. Pommier, Y. (2013) Drugging topoisomerases: lessons and challenges. *ACS Chem. Biol.* **8,** 82–95
9. Pommier, Y., and Marchand, C. (2012) Interfacial inhibitors: targeting macromolecular complexes. *Nat. Rev. Drug Discov.* **11,** 25–36
10. Wu, C. C., Li, T. K., Farh, L., Lin, L. Y., Lin, T. S., Yu, Y. J., Yen, T. J., Chiang, C. W., and Chan, N. L. (2011) Structural basis of type II topoisomerase inhibition by the anticancer drug etoposide. *Science* **333,** 459–462
11. Capranico, G., Kohn, K. W., and Pommier, Y. (1990) Local sequence requirements for DNA cleavage by mammalian topoisomerase II in the presence of doxorubicin. *Nucleic Acids Res.* **18,** 6611–6619
12. Pommier, Y., Capranico, G., Orr, A., and Kohn, K. W. (1991) Local base sequence preferences for DNA cleavage by mammalian topoisomerase II in the presence of amsacrine or teniposide. *Nucleic Acids Res.* **19,** 5973–5980
13. Cowell, I. G., Sondka, Z., Smith, K., Lee, K. C., Manville, C. M., Sidorczuk-Lesthuruge, M., Rance, H. A., Padget, K., Jackson, G. H., Adachi, N., and Austin, C. A. (2012) Model for MLL translocations in therapy-related leukemia involving topoisomerase IIβ-mediated DNA strand breaks and gene proximity. *Proc. Natl. Acad. Sci. U.S.A.* **109,** 8989–8994
14. Azarova, A. M., Lyu, Y. L., Lin, C. P., Tsai, Y. C., Lau, J. Y., Wang, J. C., and Liu, L. F. (2007) From the Cover: roles of DNA topoisomerase II isozymes in chemotherapy and secondary malignancies. *Proc. Natl. Acad. Sci. U.S.A.* **104,** 11014–11019
15. Markovits, J., Linassier, C., Fossé, P., Couprie, J., Pierre, J., Jacquemin-Sablon, A., Saucier, J.-M., Le Pecq, J. B., and Larsen, A. K. (1989) Inhibitory effects of the tyrosine kinase inhibitor genistein on mammalian DNA topoisomerase II. *Cancer Res.* **49,** 5111–5117
16. Yamashita, Y., Kawada, S., and Nakano, H. (1990) Induction of mammalian topoisomerase II dependent DNA cleavage by nonintercalative flavonoids, genistein and orobol. *Biochem. Pharmacol.* **39,** 737–744
17. Austin, C. A., Patel, S., Ono, K., Nakane, H., and Fisher, L. M. (1992) Site-specific DNA cleavage by mammalian DNA topoisomerase II induced by novel flavone and catechin derivatives. *Biochem. J.* **282,** 883–889
18. Robinson, M. J., Corbett, A. H., and Osheroff, N. (1993) Effects of topoisomerase II-targeted drugs on enzyme-mediated DNA cleavage and ATP hydrolysis: evidence for distinct drug interaction domains on topoisomerase II. *Biochemistry* **32,** 3638–3643
19. Strick, R., Strissel, P. L., Borgers, S., Smith, S. L., and Rowley, J. D. (2000) Dietary bioflavonoids induce cleavage in the MLL gene and may contribute to infant leukemia. *Proc. Natl. Acad. Sci. U.S.A.* **97,** 4790–4795
20. Lindsey, R. H., Jr., Bromberg, K. D., Felix, C. A., and Osheroff, N. (2004) 1,4-Benzoquinone is a topoisomerase II poison. *Biochemistry* **43,** 7563–7574
21. Wang, Y., Knudsen, B. R., Bjergbaek, L., Westergaard, O., and Andersen, A. H. (1999) Stimulated activity of human topoisomerases IIα and IIβ on RNA-containing substrates. *J. Biol. Chem.* **274,** 22839–22846
22. Reijns, M. A., Rabe, B., Rigby, R. E., Mill, P., Astell, K. R., Lettice, L. A., Boyle, S., Leitch, A., Keighren, M., Kilanowski, F., Devenney, P. S., Sexton, D., Grimes, G., Holt, I. J., Hill, R. E., Taylor, M. S., Lawson, K. A., Dorin, J. R., and Jackson, A. P. (2012) Enzymatic removal of ribonucleotides from DNA is essential for Mammalian genome integrity and development. *Cell* **149,** 1008–1022
23. Nick McElhinny, S. A., Watts, B. E., Kumar, D., Watt, D. L., Lundström, E. B., Burgers, P. M., Johansson, E., Chabes, A., and Kunkel, T. A. (2010) Abundant ribonucleotide incorporation into DNA by yeast replicative polymerases. *Proc. Natl. Acad. Sci. U.S.A.* **107,** 4949–4954
24. Cortes Ledesma, F., El Khamisy, S. F., Zuma, M. C., Osborn, K., and Caldecott, K. W. (2009) A human 5′-tyrosyl DNA phosphodiesterase that repairs topoisomerase-mediated DNA damage. *Nature* **461,** 674–678
25. Gao, R., Huang, S. Y., Marchand, C., and Pommier, Y. (2012) Biochemical characterization of human tyrosyl-DNA phosphodiesterase 2 (TDP2/TTRAP): a Mg^{2+}/Mn^{2+}-dependent phosphodiesterase specific for the repair of topoisomerase cleavage complexes. *J. Biol. Chem.* **287,** 30842–30852
26. Schellenberg, M. J., Appel, C. D., Adhikari, S., Robertson, P. D., Ramsden, D. A., and Williams, R. S. (2012) Mechanism of repair of 5′-topoisomerase II-DNA adducts by mammalian tyrosyl-DNA phosphodiesterase 2. *Nat. Struct. Mol. Biol.* **19,** 1363–1371
27. Shi, K., Kurahashi, K., Gao, R., Tsutakawa, S. E., Tainer, J. A., Pommier, Y., and Aihara, H. (2012) Structural basis for recognition of 5′-phosphotyrosine adducts by Tdp2. *Nat. Struct. Mol. Biol.* **19,** 1372–1377
28. Mao, Y., Desai, S. D., Ting, C. Y., Hwang, J., and Liu, L. F. (2001) 26 S proteasome-mediated degradation of topoisomerase II cleavable complexes. *J. Biol. Chem.* **276,** 40652–40658
29. Zhang, A., Lyu, Y. L., Lin, C. P., Zhou, N., Azarova, A. M., Wood, L. M., and Liu, L. F. (2006) A protease pathway for the repair of topoisomerase II-DNA covalent complexes. *J. Biol. Chem.* **281,** 35997–36003
30. Anderson, A. H., Sørensen, B. S., Christiansen, K., Svejstrup, J. Q., Lund, K., and Westergaard, O. (1991) Studies of the topoisomerase II-mediated cleavage and religation reactions by use of a suicidal double-stranded DNA substrate. *J. Biol. Chem.* **266,** 9203–9210
31. Nitiss, K. C., Malik, M., He, X., White, S. W., and Nitiss, J. L. (2006) Tyrosyl-DNA phosphodiesterase (Tdp1) participates in the repair of Top2-mediated DNA damage. *Proc. Natl. Acad. Sci. U.S.A.* **103,** 8953–8958
32. Khan, Q. A., Kohlhagen, G., Marshall, R., Austin, C. A., Kalena, G. P., Kroth, H., Sayer, J. M., Jerina, D. M., and Pommier, Y. (2003) Position-specific trapping of topoisomerase II by benzo[*a*]pyrene diol epoxide adducts: implications for interactions with intercalating anticancer agents. *Proc. Natl. Acad. Sci. U.S.A.* **100,** 12498–12503
33. Bromberg, K. D., Burgin, A. B., and Osheroff, N. (2003) A two-drug model for etoposide action against human topoisomerase IIα. *J. Biol. Chem.* **278,** 7406–7412
34. Jacob, D. A., Mercer, S. L., Osheroff, N., and Deweese, J. E. (2011) Etoposide quinone is a redox-dependent topoisomerase II poison. *Biochemistry* **50,** 5660–5667
35. Nitiss, J. L. (2009) Targeting DNA topoisomerase II in cancer chemotherapy. *Nat. Rev. Cancer* **9,** 338–350
36. Virgen-Slane, R., Rozovics, J. M., Fitzgerald, K. D., Ngo, T., Chou, W., van der Heden van Noort, G. J., Filippov, D. V., Gershon, P. D., and Semler, B. L. (2012) An RNA virus hijacks an incognito function of a DNA repair enzyme. *Proc. Natl. Acad. Sci. U.S.A.* **109,** 14634–14639
37. Clausen, A. R., Zhang, S., Burgers, P. M., Lee, M. Y., and Kunkel, T. A. (2013) Ribonucleotide incorporation, proofreading and bypass by human DNA polymerase δ. *DNA Repair* **12,** 121–127
38. Crow, Y. J., Leitch, A., Hayward, B. E., Garner, A., Parmar, R., Griffith, E., Ali, M., Semple, C., Aicardi, J., Babul-Hirji, R., Baumann, C., Baxter, P., Bertini, E., Chandler, K. E., Chitayat, D., Cau, D., Déry, C., Fazzi, E., Goizet, C., King, M. D., Klepper, J., Lacombe, D., Lanzi, G., Lyall, H., Martínez-Frías, M. L., Mathieu, M., McKeown, C., Monier, A., Oade, Y., Quarrell, O. W., Rittey, C. D., Rogers, R. C., Sanchis, A., Stephenson, J. B., Tacke, U., Till, M., Tolmie, J. L., Tomlin, P., Voit, T., Weschke, B., Woods, C. G., Lebon, P., Bonthron, D. T., Ponting, C. P., and Jackson, A. P. (2006) Mutations in genes encoding ribonuclease H2 subunits cause Aicardi-Goutieres syndrome and mimic congenital viral brain infection. *Nat. Genet.* **38,** 910–916
39. Kim, N., Huang, S. N., Williams, J. S., Li, Y. C., Clark, A. B., Cho, J. E., Kunkel, T. A., Pommier, Y., and Jinks-Robertson, S. (2011) Mutagenic processing of ribonucleotides in DNA by yeast topoisomerase I. *Science* **332,** 1561–1564
40. Williams, J. S., Smith, D. J., Marjavaara, L., Lujan, S. A., Chabes, A., and

Kunkel, T. A. (2013) Topoisomerase 1-mediated removal of ribonucleotides from nascent leading-strand DNA. *Mol. Cell* **49,** 1010–1015

41. Tumbale, P., Williams, J. S., Schellenberg, M. J., Kunkel, T. A., and Williams, R. S. (2014) Aprataxin resolves adenylated RNA-DNA junctions to maintain genome integrity. *Nature* **506,** 111–115
42. Pommier, Y., Huang, S. N., Gao, R., Das, B., Murai, J., and Marchand, C. (2014) Tyrosyl-DNA-phosphodiesterases (TDP1 and TDP2). *DNA Repair (Amst.)* 10.1016/j.dnarep.2014.03.020
43. Stoll, G., Pietiläinen, O. P., Linder, B., Suvisaari, J., Brosi, C., Hennah, W., Leppä, V., Torniainen, M., Ripatti, S., Ala-Mello, S., Plöttner, O., Rehnström, K., Tuulio-Henriksson, A., Varilo, T., Tallila, J., Kristiansson, K., Isohanni, M., Kaprio, J., Eriksson, J. G., Raitakari, O. T., Lehtimäki, T., Jarvelin, M. R., Salomaa, V., Hurles, M., Stefansson, H., Peltonen, L., Sullivan, P. F., Paunio, T., Lönnqvist, J., Daly, M. J., Fischer, U., Freimer, N. B., and Palotie, A. (2013) Deletion of TOP3β, a component of FMRP-containing mRNPs, contributes to neurodevelopmental disorders. *Nat. Neurosci.* **16,** 1228–1237
44. Xu, D., Shen, W., Guo, R., Xue, Y., Peng, W., Sima, J., Yang, J., Sharov, A., Srikantan, S., Yang, J., Fox, D., 3rd, Qian, Y., Martindale, J. L., Piao, Y., Machamer, J., Joshi, S. R., Mohanty, S., Shaw, A. C., Lloyd, T. E., Brown, G. W., Ko, M. S., Gorospe, M., Zou, S., and Wang, W. (2013) Top3β is an RNA topoisomerase that works with fragile X syndrome protein to promote synapse formation. *Nat. Neurosci.* **16,** 1238–1247
45. Chen, S. H., Plank, J. L., Willcox, S., Griffith, J. D., and Hsieh, T. S. (2014) Top3α is required during the convergent migration step of double Holliday junction dissolution. *PLoS One* **9,** e83582